International Journal of Basic and Applied Sciences, 14 (3) (2025) 373-384

International Journal of Basic and Applied Sciences

Website: www.sciencepubco.com/index.php/IJBAS
https://doi.org/10.14419/25ecam43
Research paper

Synergistic Effect of Mixed Transition Metals and Rare Earth Doping on Lithium Borate Glasses: A Structural and Optical Perspective

Anju Bishnoi [1] *, Manoj Duhan [1], Satish Khasa [2]

[1] *Department of Electronics & Communication Engineering, Deenbandhu Chhotu Ram University of Science & Technology, Murthal, Sonepat, India-131039*
[2] *Department of Physics, Deenbandhu Chhotu Ram University of Science & Technology, Murthal, Sonepat, India-131039*
**Corresponding author E-mail: 19001903002anju@dcrustm.org*

Received: July 14, 2025, Accepted: July 24, 2025, Published: July 27, 2025

Abstract

Lithium borate glasses doped with transition metal and rare earth elements have gained prominence for their tunable optical properties and diverse technological applications. In this research article, we delve into the unique contributions of key elements, dysprosium (Dy), titanium (Ti), and vanadium (V), in lithium borate glass matrices. The titanium borovandate glass system doped with Dy3+ ions with molar compositions xTiO2·(10-x)V2O5·30Li2O·60B2O3 + 1 mol% Dy2O3 glasses (with x = 0,1,3,5,9,10) have been synthesised using the melt quench technique. An extensive investigation of the structural and optical features has been carried out to evaluate the effects of titanium ions as an addition to the glass matrix. Multiple valence states of titanium (Ti3+ and Ti4+) and that of vanadium (V3+, V4+, and V5+) were unveiled through density variations and UV absorbance analysis. The shifts in bandgap have been ascertained by using a Tauc plot. Photoluminescence spectroscopy (PL) has been utilised to investigate the existence of intrinsic defects in the glass system and the influence of transition metal ions (TiO2 and V2O5) on the emission spectra. CIE chromaticity coordinates of the samples have been analysed in the white region, revealing their potential applications in display devices and optical filters.

Keywords *: Dysprosium; Photoluminescence; Titanium Dioxide; Transition Metal Ions (TMI); Y/B Ratio.*

1. Introduction

Developing advanced materials with tailored optical properties is a central research area in modern materials science and has far-reaching implications for a wide range of technological applications. Borate glasses are better glass formers than silicates and phosphates as they exhibit smaller cations, greater bond strength, and can retain non-crystallinity even at slow cooling rates. So, they can be employed as a dielectric, fast ion-conducting device, and in solid-state batteries [1], [2]. Furthermore, borate glasses containing rare earth (RE) ions are exciting materials for solid-state lighting, like white light-emitting diodes (WLEDs), vehicle indicators, display devices, etc. [3] as they possess remarkable RE ion solubility[4]. The borate glass structure consists of only two types of structural units, i.e., BO_3 and BO_4 units. The interconvertibility of these two units strongly depends upon the ratio of the glass modifier, such as alkali oxides [5]. Lithium borate glasses have emerged as promising candidates among these materials due to their transparency, good chemical durability, and the ease with which they can be tuned to exhibit specific optical characteristics. In particular, incorporating different dopants into the glass matrix allows for precise control over their optical behaviour, making them appealing for applications in photonics, optical sensors, laser systems, and optical communications [6].

Lanthanide ions can activate borate glassy matrices, allowing for even more fine-tuning of luminescence properties [7]. Among the lanthanides, dysprosium is a reliable material for luminescence studies. Luminescence spectra of dysprosium ions (Dy^{3+}) consist of significant visible emission (in the yellow and blue regions) under UV excitation. The transitions involved are $^4F_{9/2} \rightarrow {}^6H_{15/2}$ (blue color) and $^4F_{9/2} \rightarrow {}^6H_{13/2}$ (yellow color), which could potentially generate white light[8]. The key challenge for researchers is to fine-tune the ambient field of Dy^{3+} ion-activated glassy matrices to create white luminescence with the appropriate yellow-to-blue (Y/B) intensity ratio[9].

Borate glasses doped with transition metal ions (TMI) are suitable for numerous applications like solid-state lasers and solar energy converters[10–12]. The glass characteristics get modified in the presence of TMI in the glass matrix, as variable transition states may form different structural units. There are several studies in which incorporating vanadyl ions (VO^{2+}) leads to changes in the chemical bonds and structural rearrangements occur in the glass system, thereby altering the optical behaviour of the glasses[4,13–15]. Titanium dioxide (TiO_2) is added to the glass matrix as it may enhance the optical and electrical characteristics [6]. Titanium ions may act as a glass modifier (Ti^{3+}/TiO_6) as well as a glass former (Ti^{4+}/TiO_8) due to their low coordination numbers[16–18]. Additionally, TiO_2 is considered a non-

toxic and low-cost n-type semiconductor[19]. Recently, B. Tirumala Rao et al. reported the spectral investigations of TiO_2-doped zinc alumino lithium borate glasses[20]. Vishab Kesarvani et al. studied the impact of incorporating TiO_2 as a modifier in tellurium tungstate glasses and found that titanium ions caused major structural changes and enhanced the photoluminescence (PL) emission[21]. B. Srinivas et al. examined the effect of V_2O_5 on strontium titanium boro-tellurite glasses and found that the optical absorption spectra were dominated by VO^{2+} ions transitions[22]. S. Cetinkaya Colak reported the role of TiO_2 in improving the structural and optical characteristics of zinc borate glasses when added in small amounts[23]. B.V. Padlyak et al. studied the luminescence of lithium tetraborate glasses co-doped with manganese and europium and found their emission in the orange-red region [24]. P. Sai Dinesh et al. examined the impact of different modifiers on Dy^{3+} doped lithium tetraborate glasses [25]. S. Karthika et al. studied the vanadium-doped lithium telluro-borate glasses and investigated the compactness of the structure and decrease in direct optical bandgap with the addition of vanadium ions [26]. Sonam Raheja et al. examined the titanium-doped niobium borate glasses and found a red shift in the cut-off wavelength and a decrease in the optical band gap values with decreasing Nb_2O_5 content [27].

Therefore, it is worthwhile to investigate the impact of substituting one intermediate oxide, V_2O_5, with another intermediate oxide, TiO_2, on the structural and optical properties of polynary glasses because the synergistic effect of all the participating ions results in highly flexible properties for this multicomponent glass system. Thus, the authors intend to understand the mechanisms underlying the observed results by extensively examining structural and optical features. Understanding these interactions is essential for harnessing the full potential of lithium borate glasses for advanced optical applications and tailoring their properties to meet specific technological requirements.

2. Materials and methodology/ experimental details

Glasses with the chemical composition $x TiO_2 \cdot (10\text{-}x)\ V_2O_5 \cdot 30Li_2O \cdot 60B_2O_3$ + 1 mol% Dy_2O_3 glasses (with x = 0,1,3,5,9,10) have been prepared using melt quenching method. The sample codes and the chemical composition are mentioned in Table 1. AR grade chemicals of lithium carbonate (Li_2BO_3 with 99.5% purity), boric acid (H_3BO_3 with 99.5% purity), titanium dioxide (TiO_2 with 99% purity), vanadium oxide (V_2O_5 with 99% purity), and dysprosium oxide (Dy_2O_3 with 99.9% purity) of make Hi-media have been used for glass synthesis. The detailed synthesis procedure is shown in Fig. 1(a). The prepared glass samples (as shown in Fig. 1 (b)) have been optically polished and ground into fine powder to investigate different characterizations. X-Ray diffraction (XRD) profile obtained from an X-ray diffractometer (Rigaku Model Ultima IV) employing Cu-K_α (X-Rays with λ=0.154 nm) exposure to samples at 30 kV applied voltage, anode current of 15 mA, and having angle (2θ) variation from 15°-80° has confirmed the amorphous character of the glass samples. Density has been calculated by Archimedes' principle using an organic buoyant liquid, xylene. The KBr pellet approach has been used to record Fourier Transform Infrared (FTIR) spectra at room temperature (RT) using an FTIR spectrophotometer (Perkin Elmer's with a resolution of 1 cm^{-1}) in the mid-IR range of 4000-400 cm^{-1} for structural analysis. By mixing the sample with KBr in a mass ratio of 1:100, the resultant mixture has been processed into pellets. A UV-Vis spectrometer (Shimadzu UV3600) has been used to record the absorption spectra of the polished glass samples at RT in the 200-1800 nm wavelength range with 0.1 nm resolution. PL spectra recorded with a Horiba spectrometer (Fluoromax R298P) in the 200-800 nm wavelength range (using a Xenon lamp as an excitation source) have been used to analyse the luminescence characteristics. The excitation and emission spectral slit widths are both set at 3 nm.

Table 1: Composition of $x TiO_2 \cdot (10\text{-}x)\ V_2O_5 \cdot 30Li_2O \cdot 60B_2O_3$ + 1 mol% Dy_2O_3 Glasses (with x = 0,1,3,5,9,10)

S. No.	Chemical composition	Glass code	Appearance
1.	$10V_2O_5 \cdot 30Li_2O \cdot 60B_2O_3$ + 1 mol% Dy_2O_3	TLVBD0	Dark brown
2.	$TiO_2 \cdot 9V_2O_5 \cdot 30Li_2O \cdot 60B_2O_3$ + 1 mol% Dy_2O_3	TLVBD1	Dark brown
3.	$3TiO_2 \cdot 7V_2O_5 \cdot 30Li_2O \cdot 60B_2O_3$ + 1 mol% Dy_2O_3	TLVBD3	Light brown
4.	$5TiO_2 \cdot 5V_2O_5 \cdot 30Li_2O \cdot 60B_2O_3$ + 1 mol% Dy_2O_3	TLVBD5	Light brown
5.	$9TiO_2 \cdot V_2O_5 \cdot 30Li_2O \cdot 60B_2O_3$ + 1 mol% Dy_2O_3	TLVBD9	Light green
6.	$10TiO_2 \cdot 30Li_2O \cdot 60B_2O_3$ + 1 mol% Dy_2O_3	TLVBD10	Transparent

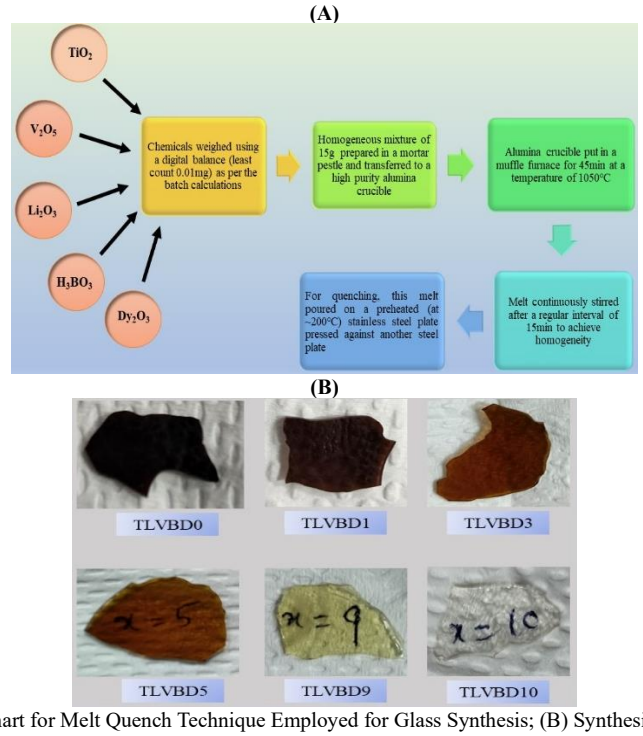

Fig. 1: A) Flow Chart for Melt Quench Technique Employed for Glass Synthesis; (B) Synthesised Glass Samples.

3. Results and discussion

3.1. XRD investigation

Fig. 2 shows the X-ray diffractograms of the TLVBD glass system. The XRD patterns exhibit broad diffusion humps but no discernible crystalline phases. The complete absence of any peaks in the diffractogram reflects the non-crystalline character of the glass samples. All the samples have shown broad halos at lower scattering angles (15°–30°), depicting the non-existence of long-range atomic orders and thus confirming the amorphous nature of the prepared glass series.

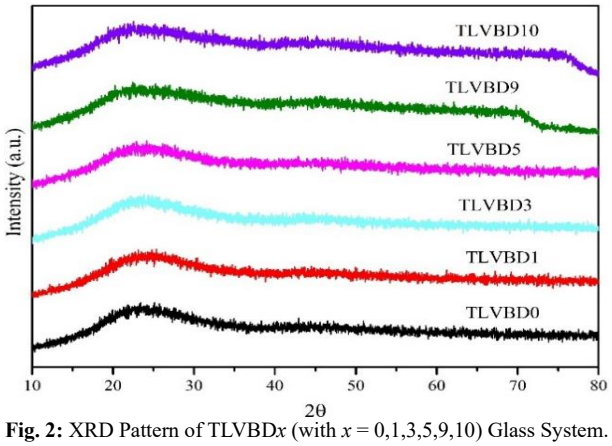

Fig. 2: XRD Pattern of TLVBD*x* (with *x* = 0,1,3,5,9,10) Glass System.

3.2. Physical parameters

For investigating the structural changes in the developed glass system, different parameters (tabulated in Table 2) have been estimated by using formulas from the literature[28–31]. The density of the glass system is dependent on the molecular mass and volume of the prepared glass samples. As given in Table 2, the density of the TLVBD glasses has increased initially, depicting the compactness of the glass structure as TiO_2 is introduced in the glass matrix. It may be due to the possibility of vanadium ions ($V^{3+}/V^{4+}/V^{5+}$) existing in octahedral coordinated form initially, and with the introduction of titanium ions (probably in Ti^{4+} state), the structure reduced to a 4-coordinated tetrahedral form. Thereafter, as the amount of TiO_2 is slightly increased from 1 mol% to 3 mol%, the density decreases. There may be two probable possibilities for this decrement; one is the heavier V_2O_5 (mol. wt. = 181.88 g/mol) has been substituted with the lighter TiO_2 (mol. wt. = 81.38 g/mol) and the other being titanium ions reduction from Ti^{4+} (ionic radius = 0.056 nm) state to Ti^{3+} state (ionic radius = 0.081 nm) which is comparable in size to ionic radii of vanadium ions (0.078 nm). As the content of V_2O_5 is further replaced by TiO_2 (from 5 mol% to 10 mol%), the density values show an increasing trend again, indicating the structure compactness with TiO_2 enhancement. Although the molecular weight of the glass system is decreasing but the volume is also shrinking at a higher rate, depicting the structural modifications due to the major changes in the coordination number of the neighbouring ions. This decreasing volume may be a result of the decreasing inter-ionic distance of titanium ions as reported in Table 2. Additionally, the decrease in inter-ionic distance (r_i) and polaron radius (r_p) resulted in greater Ti-O bond strength, leading to stronger field strength around titanium ions [4], [32].

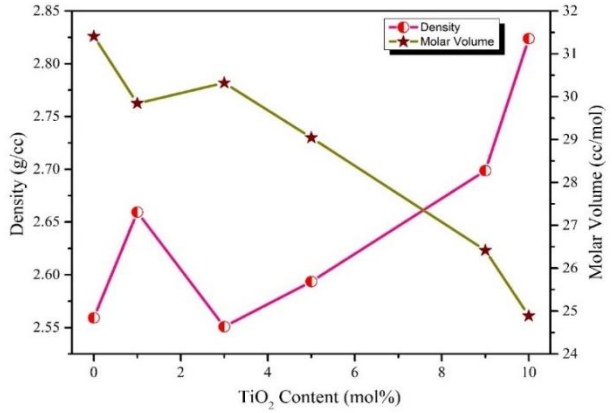

Fig. 3: Density and Molar Volume Variations of TLVBD*x* (with *x* = 0,1,3,5,9,10) Glasses with TiO_2 mol%.

Table 2: Summary of Different Physical Parameters of $xTiO_2 \cdot (10\text{-}x)\ V_2O_5 \cdot 30Li_2O \cdot 60B_2O_3$ + 1 mol% Dy_2O_3 Glasses (with *x* = 0,1,3,5,9,10)

Physical Parameters	Glass codes TLVBD0	TLVBD1	TLVBD3	TLVBD5	TLVBD9	TLVBD10
Molecular Weight(g/mol)	80.38	79.37	77.35	75.33	71.29	70.28
Density (ρ) (g/cc) (±0.02)	2.56	2.65	2.55	2.59	2.69	2.82
Molar Volume (V_m) (cc/mol)	31.41	29.85	30.32	29.04	26.42	24.89
Titanium Ion concentration(N_i) (ion/cm^3)x10^{21}	-	0.20	0.59	1.03	2.03	2.39
Inter-ionic distance (r_i)x10^{-7}	-	1.71	1.19	0.99	0.79	0.75
Polaron radius (r_p)x10^{-7}	-	0.69	0.48	0.40	0.32	0.30
Field strength (10^{14} cm^{-2})	-	4.21	8.66	12.53	19.75	22.04
N_4 value	0.43	0.47	0.37	0.39	0.61	0.79

3.3. Fourier transform infrared spectroscopy (FTIR)

FTIR spectroscopy reveals the rotations linked to a covalent bond as well as the existing molecular vibrations, thereby giving information about the different structural units present in the glass structure. The FTIR spectra for the doped glass samples shown in Fig. 4 have been recorded in the range of 400-2000 cm^{-1}. The broad bands existing in the absorbance spectra confirm the amorphous nature of the glasses[33–36].

The spectra in Fig. 4 exhibited all the three main absorption regions of vitreous borate glasses: (i) ~600-800 cm^{-1} (due to the tilting of B-O-B links in triangular BO_3 units), (ii) ~800-1200 cm^{-1} (due to the B-O stretching of tetrahedral BO_4 units) and (iii) ~1200-1600 cm^{-1} (because of the B-O stretching in triangular BO_3 units) [37], [38]. It can be seen clearly that, as the concentration of titanium ions increases, the bands are broadened. To identify the exact peak positions in this broad spectrum, we have deconvoluted these with the help of Gaussian multiple peak fitting in OriginPro 9. Fig. 5 represents the deconvoluted spectra of sample TLVBD5 with a coefficient of correlation (R^2) being 0.999.

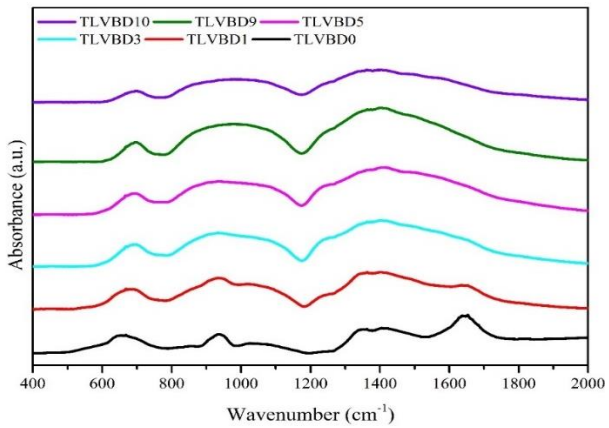

Fig. 4: Fourier Transform Infrared Spectra Observed for TLVBD Glass Matrix in the Range 400-2000 cm^{-1}.

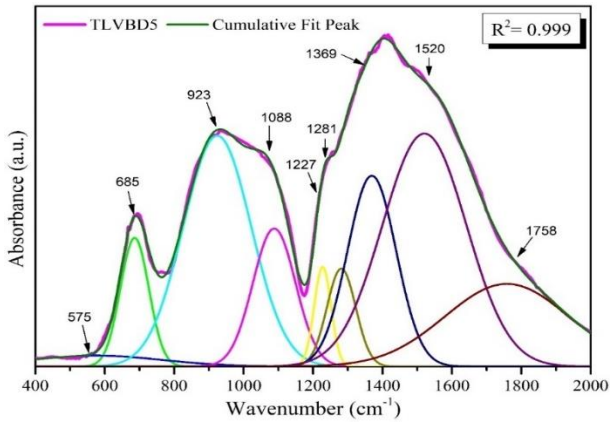

Fig. 5: Deconvoluted FTIR Spectra (by Gaussian Multiple Peak Fitting) of Sample TLVBD5.

The incorporation of titanium ions in different ratios in the prepared glass matrix has led to the following modifications: -

1) In the deconvoluted FTIR spectrum, the band originating around 575 cm^{-1} might be ascribed to the vibrations of Li^+ ions [2] and the Ti-O bond in octahedral TiO_6 groups[39].
2) The band peak positioned at ~685 cm^{-1} substantiates the presence of B-O-B tilting vibration of triangular borate (BO_3) groups[38]. It can be observed from Fig. 4 that this band is getting sharpened in samples TLVBD1-TLVBD9 at a concentration of titanium ions from 1 mol% to 9 mol%, whereas the intensity drops at 10 mol%. Also, its position gets shifted to a higher wave number from 670 cm^{-1} (TLVBD0) to ~692 cm^{-1} (TLVBD10). This results from distorted B-O linkage vibrations in the glass structure and indicates the presence of B-O-Ti linkages vibrations of the TiO_4 group at tetrahedral and octahedral positions of the glass structure, thus revealing major modifications in the glass network with the addition of TiO_2 [37], [40], [41].
3) The peak centered at ~923 cm^{-1} in sample TLVBD5 is the result of stretching vibrations of the B-O bond in different BO_4 units in tri, tetra and penta-borate groups[1,42] and V=O vibration of vanadium group (VO_5)[43]. This peak is highly intense in sample TLVBD0 (in Fig. 4), whereas it is suppressed on the addition of titanium ions in the glass matrix.
4) The band around ~1088 cm^{-1} and ~1227 cm^{-1} occurred because of less intense boron-oxygen stretching of non-bridging oxygens (NBOs) in BO_4 vibrations due to tri-borate, tetra-borate, and penta-borate groups, thus resulting in 4-coordinated boron units [40], [41].
5) The peaks around 1281 cm^{-1} and 1369 cm^{-1} are the consolidated effect of stretching vibrations of B(III)-O-B(IV) of BO_3-O-BO_4 and B-O linkage of $(BO_3)^{3-}$ group in orthoborate and meta-borate chains, respectively [4,40].
6) The absorption band around 1520 cm^{-1} is due to the stretching vibrations in B-O^- of BO_3 units and BO_3 units having 1 non-bonding oxygen and 2 bonding oxygen linked with tetraborate units [38], [46], [47] and the peak at ~1758 cm^{-1} can be assigned to the vibrations of OH^- ions [39].

3.4. UV-Vis-NIR absorption study

The optical features of the TLVBD glass system were examined through UV-Vis-NIR absorption spectroscopy, as shown in Fig. 6. This method involves the absorption of photons with energy higher than the optical band gap. The UV-Vis-NIR absorption spectra for the

TLVBD*x* (with *x* = 0,1,3,5,9,10) glass system shown in Fig. 6 were recorded between 280 nm and 2200 nm wavelength range. The amorphous nature of glasses was ascertained by the absence of a sharp absorption edge. Ten absorption bands were detected at ~ 392 nm, 450 nm, 748 nm, 800 nm, 906 nm, 1096 nm, 1274 nm, 1430 nm, 1676 nm, and 1943 nm corresponding to Dy^{3+} ions. These bands corresponded to the transitions originating from ground state $^6H_{15/2} \rightarrow {}^4F_{7/2}$, $^4I_{15/2}$, $^6F_{3/2}$, $^6F_{5/2}$, $^6F_{7/2}$, $^6H_{7/2}$, $^6F_{11/2} + {}^6H_{9/2}$, $^6H_{9/2}$, $^6H_{11/2}$ respectively [48]. These transitions were marked as per the assignments published by W.T. Carnall et al. [49]. The absorption bands at ~392 nm in the UV region and ~ 450 nm in the visible region were only exhibited by the glass sample TLVBD10. These were absent in all other samples doped with vanadium as seen in our previous results, except TLVBD9, exhibiting a very less intense band at ~ 748 nm [4]. This might be due to the increase in absorption in the UV-Vis region with vanadium doping, and so the transitions were forbidden by spin selection rules. These observations suggested that titanium ions have very less impact on absorption in the UV-Vis region as compared to vanadium ions. The peaks observed in the near-infrared (NIR) region in Fig. 6 are comparatively broader and more intense than in the visible region.

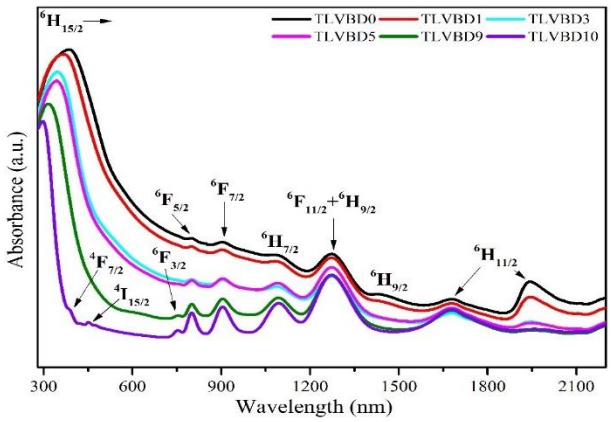

Fig. 6: Optical Absorption Spectra of TLVBD*x* (with *x* = 0,1,3,5,9,10) Glasses in the Wavelength Range 280 nm-2200 nm.

3.4.1. Nephelauxetic effect

There has been a displacement in wavenumber of transitions in the glass system concerning aqua ion positions due to deformation in 4f orbitals of Dy^{3+} ions, identified as nephelauxetic effect. It anticipates the hypersensitive nature and covalent character of Dy^{3+}-O bonding in the glass matrix. The covalency causes a decrease in interelectronic repulsion. The band at ~1274 nm occurred due to $^6H_{15/2} \rightarrow {}^6F_{11/2}$ transition is hypersensitive as its width and intensity vary with the surroundings of dysprosium ions [50] and is allowed by selection rules $||\Delta S|| = 0$, $||\Delta L|| \leq 2$ and $||\Delta J|| \leq 2$ [28], [46]. Average Nephelauxetic ratio $\overline{(\beta)}$ and bonding parameter (δ) were calculated as per mathematical formulas reported in literature [4], and the obtained values are tabulated in Table 3. The bonding parameter (δ) values are found to be positive, depicting the covalent character of the bond shared by Dy^{3+} ions with the surrounding ligands. Due to this covalent Dy^{3+}-O bonding, stronger asymmetry exists in the ligand field environment around Dy^{3+} ions that governs the probabilities of electronic transitions responsible for light emission, thereby directly impacting the optical intensity and efficiency in white light production [51].

3.4.2. Absorption edge, optical band gap, and Urbach energy analysis

Cut-off wavelength ($\lambda_{cut\text{-}off}$) was determined by linear fitting of the absorption edge of absorption spectra, as shown in Fig. 7, and values were reported in Table 3. It shows a decreasing trend with increasing amount of titanium ions in the glass matrix. This might be either due to the absence of major change in electronic transitions in the UV-Vis region due to Ti^{4+} ions that caused the blue-shifted absorption edge, or possibly TiO_2 is behaving as a glass former, enhancing network connectivity, leading to fewer NBOs that caused a decrease in cut-off wavelength [52]. This was also reflected by the FTIR results (increase in N_4 value with increasing content of titanium oxide).

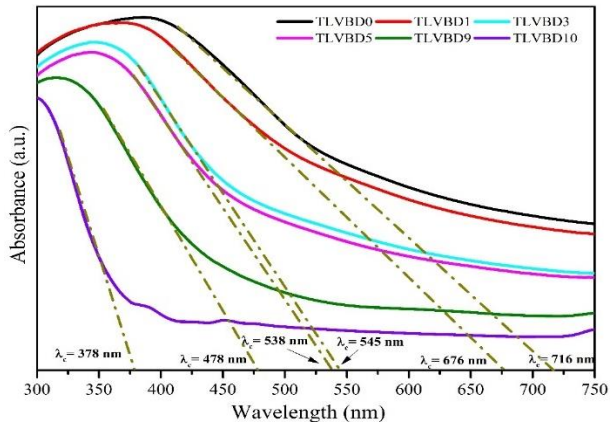

Fig. 7: Cut-Off Wavelength of TLVBD Glass System by Extrapolating the Absorption Edge in 300 nm-750 nm Wavelength Range.

Generally, in amorphous solids, indirect transitions across the optical band gap define the optical absorption edge [53]. Optical band gap of the TLVBD glass matrix was ascertained by the theory given by Mott and Davis relating the absorbance coefficient (α) to the incident photon energy (hν) given below [4], [28]:

$$\alpha = b\frac{(h\nu - E_g)^r}{h\nu} \quad (1)$$

Where b is the band tailing parameter and r is a constant based on the type of electronic and optical transitions. There is a possibility of only indirect (allowed and forbidden) transitions in case of glasses due to their amorphous nature, so r = 2 (for indirect allowed transitions) and r = 3 (for indirect forbidden transitions). The indirect optical band gap (E_g) values were evaluated by drawing a graph of $(\alpha h\nu)^{1/2}$ versus photon energy ($h\nu$) and extending the linear region of the y-axis to meet at the x-axis, as shown in Fig. 8 and reported in Table 3. These values varied non-linearly between 0.63 eV and 2.86 eV for r = 2 and between 0.052 eV and 2.43 eV for r = 3. The lower band gap values hinted at the low-energy semiconducting behaviour of the glass matrix due to the high probability of thermally activated conduction, thus bridging the gap between insulators and traditional semiconducting materials. The non-linear variations in the band gap were possibly due to the combined effect of TiO_2 and V_2O_5 in this multi-component glass system. Initially, when 1 mol% TiO_2 is introduced in the Dy^{3+} doped boro-vandate glass (sample TLVBD1), the band gap decreased slightly, possibly due to the formation of oxygen vacancies within the band gap that acted as intermediate energy states and reduced the gap [54]. Thereafter, it increased up to 3 mol% and then showed a very less diminishing effect up to 5 mol% of TiO_2, as vanadium ions have a higher positive charge and smaller radius as compared to titanium ions, thus possessing a strong polarization effect on oxygen ions [55]. Between 5-10 mol% of titanium content, the share of vanadium ions' effect seems to be diminishing and the band gap goes on increasing. Glass samples TLVBD0, TLVBD1, TLVBD3, TLVBD5 and TLVBD9 have optical band gap <1.7 eV, implying they can absorb infrared (IR) and near-IR light making them suitable candidates for application in the areas of IR sensors, thermal imaging and night vision.

Refractive index (η) is another parameter useful for investigating the optical features and the compatibility of the glassy material in various areas. It depends on coordination no. of ion, electronic polarizability of the oxide ion and polarizability of the directly connected neighbour ions [48]. The values of refractive index were calculated using the following formula given by Dimitrov and Sakka [48], [52] and are reported in Table 3:

$$\frac{\eta^2-1}{\eta^2+2} = 1 - \sqrt{\frac{E_g}{20}} \tag{2}$$

Molar refractivity (R_m), electron polarizability (α_m) and optical dielectric constant (ε) were also determined by using the formulas from literature [48] and their values were reported in Table 3. It was found out that molar refractivity and polarizability decreased with the increasing content of titanium ions as there were fewer NBOs as the amount of TiO_2 increased in the glass system.

Table 3: Cut-Off Wavelength($\lambda_{cut\text{-}off}$), Optical Band Gap (E_g), Urbach Energy (ΔU), Nephelauxetic Ratio $\overline{(B)}$, Bonding Parameter (δ), Refractive Index (η), Two Photon Absorption Coefficient (β_{TPA}), Molar Refractivity (R_m), Electron Polarizability (α_m) and Dielectric Constant (ε) of TLVBD Glass Matrix

Parameters	TLVBD0	TLVBD1	TLVBD3	TLVBD5	TLVBD9	TLVBD10
$\lambda_{cut\text{-}off}$ (nm)	716	676	545	538	478	378
E_g (r=2) eV	0.72	0.63	1.54	1.47	1.89	2.86
E_g (r=3) eV	0.085	0.052	0.8	0.72	1.15	2.43
ΔU	1.282	1.437	0.976	1.002	0.757	0.450
$\overline{(\beta)}$	0.979	0.990	0.991	0.989	0.991	0.992
δ	2.09	1.01	0.88	1.10	0.84	0.86
η	3.72	3.86	2.97	3.01	2.79	2.44
β_{TPA}	30.93	31.66	24.29	24.85	21.45	13.59
R_m	25.45	24.55	21.91	21.17	18.30	15.48
α_m x 10^{-24}	10.08	9.73	8.68	8.39	7.25	6.13
ε	13.81	14.90	8.81	9.07	7.76	5.93

In the optical absorption spectrum, the exponential tail of the absorption edge is characterized by Urbach energy (ΔU). In glassy materials, the degree of disorder and defect states is reflected by the Urbach energy that was determined by the following relation:

$$\alpha = \alpha_o e^{\frac{h\nu}{\Delta U}} \tag{3}$$

ΔU values were evaluated by linear fitting the absorption coefficient ln(α) versus energy of photon ($h\nu$) to an exponential function as shown in Fig. 9, and taking the inverse of the slope values thus obtained. The calculated values of Urbach energy are reported in Table 3. These values are found to be high, indicating that TLVBD glass matrix has better possibilities to modify the weak bonds into structural disorders and internal defects. Moreover, these values were found to follow an opposite trend concerning band gap, suggesting more localized states within the gap [51].

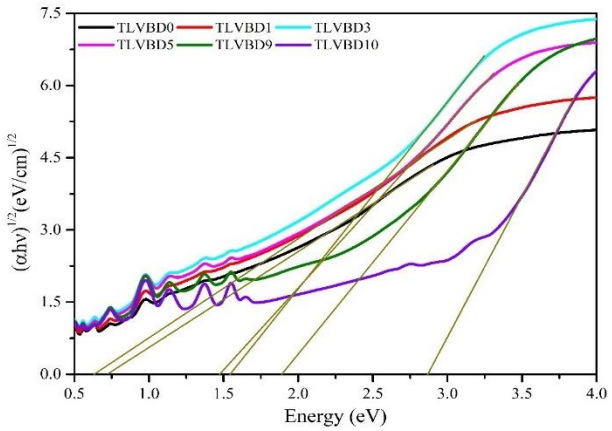

Fig. 8: Tauc's Plot for TLVBD*x* (with *x* = 0,1,3,5,9,10) Glass Matrix with r =2 and extrapolation indicates the Indirect Band Gap.

To estimate the optical switching performance in waveguides, the photon absorption (TPA) coefficient (β_{TPA}) is a very important factor. It quantifies how effectively a material absorbs light through the simultaneous absorption of two photons and was determined by the following relation [44]:

$$\beta_{TPA}(\text{cm/Gigawatt}) = 36.76 - 8.1E_g \quad (4)$$

The calculated values of β_{TPA} are reported in Table 3, and the TLVBD10 glass sample has the lowest value (13.59 cm/GW) of $\beta_{TPA,}$ hinting its utility in waveguides [44].

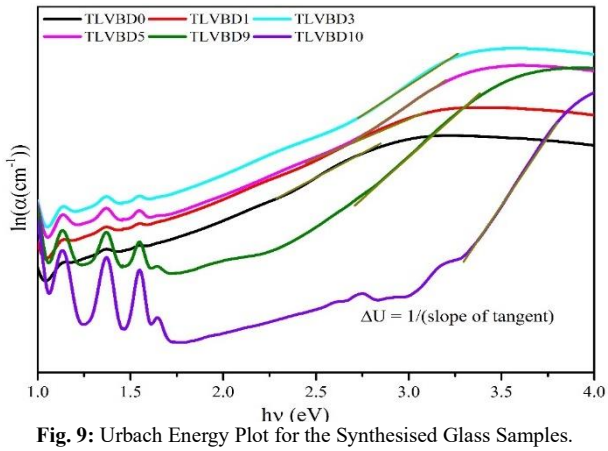

Fig. 9: Urbach Energy Plot for the Synthesised Glass Samples.

3.5. Photoluminescence (PL) investigation

3.5.1. Emission and excitation spectra

PL spectra (as shown in Figs 10 and 11) were recorded for the synthesised glass samples to investigate the dynamics of luminescence and energy levels generated due to the Dy^{3+} ions through the luminescence mechanism. The excitation spectra as demonstrated in Fig. 10 was monitored at an emission wavelength λ_{em} = 577 nm corresponding to Dy^{3+} ions in the spectral range 300-550 nm. It disclosed eight excited bands for 4f-4f transitions of trivalent dysprosium ions centered at ~ 324 nm ($^6H_{15/2} \rightarrow {}^6P_{3/2}$), ~350 nm ($^6H_{15/2} \rightarrow {}^6P_{7/2}$), ~363 nm ($^6H_{15/2} \rightarrow {}^6P_{5/2}$), ~386 nm ($^6H_{15/2} \rightarrow {}^4F_{7/2}$), ~424 nm ($^6H_{15/2} \rightarrow {}^4G_{11/2}$), ~452 nm ($^6H_{15/2} \rightarrow {}^4I_{15/2}$), ~472 nm ($^6H_{15/2} \rightarrow {}^4F_{9/2}$) and ~527 nm ($^6H_{15/2} \rightarrow {}^6F_{3/2}$) [4]. Among these transitions, the four most intense transitions were chosen for exploring the emission spectra.

The luminescence spectral profile in Fig. 11 demonstrated that there was emission of one intense blue region band centered at 482 nm (corresponding to $^4F_{9/2} \rightarrow {}^6H_{15/2}$), another more intense yellow region band centered at 574 nm (corresponding to $^4F_{9/2} \rightarrow {}^6H_{13/2}$) and a feeble red region band centered at 664 nm (corresponding to $^4F_{9/2} \rightarrow {}^6H_{11/2}$) for excitation wavelengths λ_{exc} = 350 nm and 452 nm, ascribed to the characteristic intra f-f transitions of trivalent dysprosium ions [56].

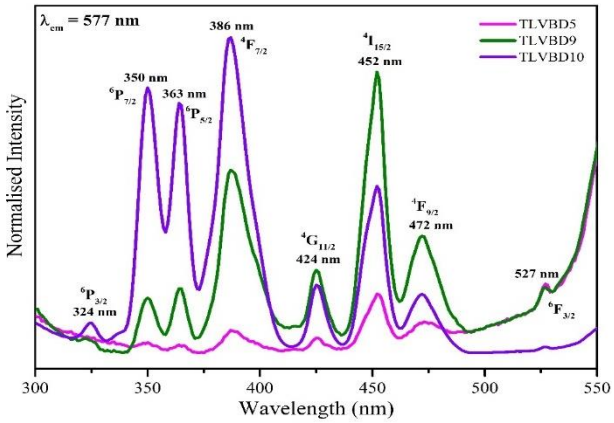

Fig. 10: PL Excitation Spectra of 1 mol% Dysprosium-Doped TLVBD*x* (with *x* =5,9,10) Glass Matrix with Emission Wavelength of 577 nm.

Along with these bands, there existed a weak band centered at 693 nm (corresponding to $^2E \rightarrow {}^2T_2$ transition of Ti^{3+} ions [57]) for λ_{exc} = 363 nm, which got shifted to 733 nm for λ_{exc} = 386 nm, indicating the presence of titanium ions in Ti^{3+} valence state for 5mol% -10 mol% concentration of TiO_2 in the synthesised glass samples. The $^6H_{15/2}$ transition (blue band) is a magnetic dipole (MD) transition ($\Delta J = 0, \pm 1$ but $0 \leftrightarrow 0$ forbidden) that is not affected by the surrounding environment of Dy^{3+} ions. The yellow band ($^6H_{13/2}$) is an electronic dipole (ED) transition (permitted by the selection rule $\Delta S = 0$, $\Delta L = 2$, $\Delta J = 2$) and is hypersensitive, being sensitive to the pristine glass environment [32]. The intensity ratio of ED to MD (Yellow/Blue or Y/B ratio) is used to explore the local environment around Dy^{3+} ions and lattice symmetry in the host glass matrix. Generally, the interaction of RE ions with the host glass is determined by its degree of symmetry. More is symmetry in the host glass system, the less is the interaction among the RE ions and the host, and vice-versa. As shown in Fig.12, the Y/B ratio is observed to be high (>1) except for 452 nm excitation wavelength, indicating an asymmetric environment around Dy^{3+} ions in the synthesised host lattice as well as the ability of the Dy^{3+} ions to produce white light in the TLVBD glass system [56].

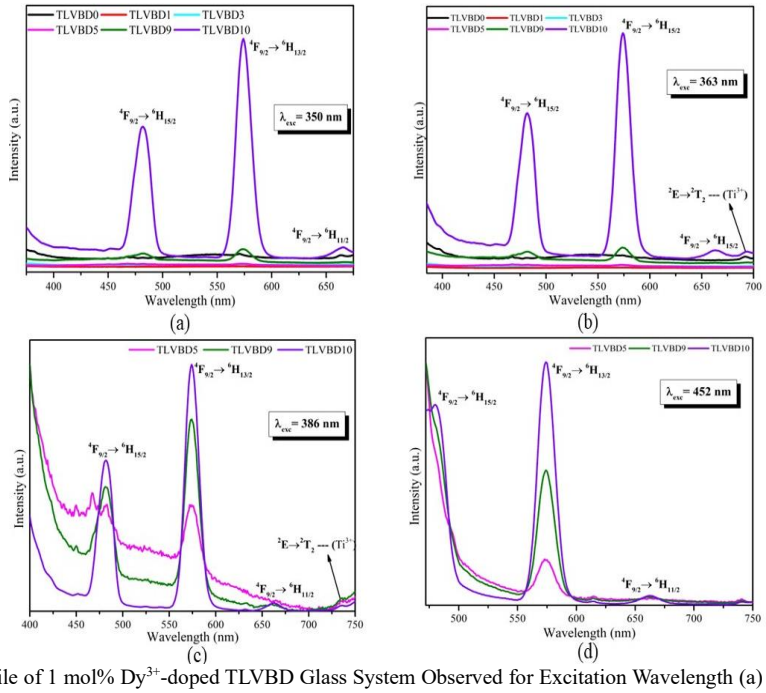

Fig. 11: Emission Spectral Profile of 1 mol% Dy^{3+}-doped TLVBD Glass System Observed for Excitation Wavelength (a) 350 nm, (b) 363 nm, (c) 386 nm, (d) 452 nm, respectively.

Fig. 12 also suggested that the Y/B ratio has a strong dependence on the amount of TiO_2 and V_2O_5 in the glass matrix. As per the results of our previous work [4], vanadium concentration significantly reduces the intensity of the yellow band and enhances the intensity of the blue band. This was also reflected in the TLVBD glass system when sample TLVBD10 (with 0 mol% of vanadium) exhibited a sharp increase in the intensity of both the bands along with a high Y/B ratio, indicating that titanium ions enhance the luminescence due to Dy^{3+} ions by generating more asymmetry in the lattice. PL emission is also significantly affected by the wavelength of excitation. This is depicted in Fig. 12 for λ_{exc} = 452 nm; the low values of Y/B ratio may be due to possibly more excitation into the energy levels, favouring the blue emission.

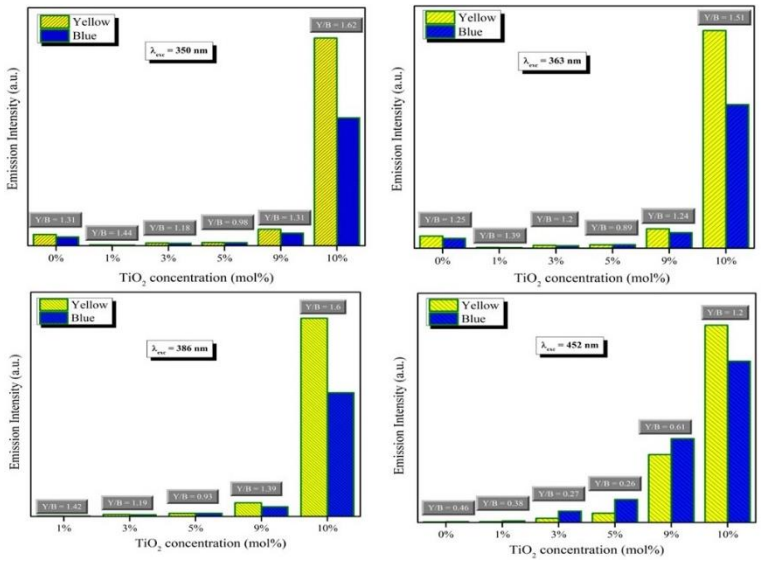

Fig. 12: Comparison of Y/B Ratio for TLVBD Glass System with the Increasing Concentration of TiO_2 at Excitation Wavelengths of 350 nm, 363 nm, 386 nm, and 452 nm, depicting increasing Asymmetry in the Lattice.

3.5.2. Energy level diagram

Fig. 13 depicts the schematic energy level diagram of trivalent dysprosium ions. Initially, the Dy^{3+} ions lying in the ground state were stimulated to different higher energy levels through absorption of excitation wavelengths at 350 nm, 363 nm, 386 nm, and 452 nm. As the energy levels above $^4F_{9/2}$ level had less energy difference, the Dy^{3+} ions tended to decay non-radiatively from those higher energy levels to $^4F_{9/2}$ metastable state, causing a population explosion at this level. Contrary to this, there was the least probability for a non-radiative transition from $^4F_{9/2}$ to $^6F_{3/2}$ state due to an appreciable energy difference between them. So, Dy^{3+} ions relax radiatively to lower energy states emitting light at 482 nm (in blue region), 574 nm (in yellow region), and 664 nm (in red region) as shown in Fig. 13. Pristine glass matrix, chemical composition, and pumping wavelength were some factors that decided the feasibility of these transitions [4], [32]. As depicted in Fig.13, there were probable chances of energy transfer between two Dy^{3+} ions non-radiatively due to cross relaxation (CR), which occurred due to energy transfer from excited state Dy^{3+} ions to the ions lying in the nearby ground state. It caused both the ions to be in an intermediate state and dissipate energy to the ground state non-radiatively [48].

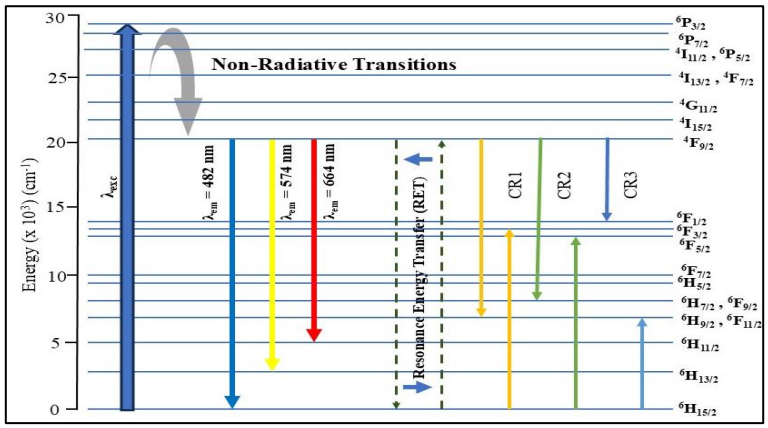

Fig. 13: Schematic Energy Level Diagram of Trivalent Disprosium Ions.

3.5.3. Colorimetric analysis

Colorimetry (or "science of color") is the scrutiny of colors emitted by a material, so its insight is often blended with human color vision. Practically, the human eye perceives the fusion of two colors as a single color and is usually imperceptible to an authentic dichromatic composition of that fusion [58]. Hence, to ascertain the colorimetry evaluation of the TLVBD glass matrix, the chromaticity coordinates (x,y) and color correlated temperature (CCT) were estimated using the Commission Internationale de l'Eclairage (CIE) – 1931 system. For color matching of the spectral distribution, P(λ) of the synthesised glass samples, three tristimulus functions X, Y, and Z were determined using the relations as follows [32]:

$$X = \int_{\lambda}^{0} \bar{x}(\lambda)P(\lambda)d\lambda \quad (5)$$

$$Y = \int_{\lambda}^{0} \bar{y}(\lambda)P(\lambda)d\lambda \quad (6)$$

$$Z = \int_{\lambda}^{0} \bar{z}(\lambda)P(\lambda)d\lambda \quad (7)$$

$\bar{x}(\lambda), \bar{y}(\lambda)$ and $\bar{z}(\lambda)$ were standard color matching functions of the 1931 CIE system, and dλ represented a very narrow bandwidth for executing the simulation. The Tristimulus function values (X, Y, Z) are then estimated from the CIE chromaticity coordinates (x, y, z) using the following formulae:

$$x = \frac{X}{X+Y+Z} \quad (8)$$

$$y = \frac{Y}{X+Y+Z} \quad (9)$$

$$z = \frac{Z}{X+Y+Z} \quad (10)$$

The obtained values were compiled in Table 4. Fig. 14 illustrates these color coordinates (x,y) for 1 mol% Dy^{3+}-doped TLVBD glass matrix for different excitation wavelengths. The standard white luminescence value (0.33, 0.33) lies in the centre of the diagram. For λ_{exc} = 350 nm, 363 nm, and 386 nm, the obtained color coordinates are quite close to the standard white light, and for λ_{exc} = 452 nm, the color coordinates shifted to longer wavelengths, matching the yellowish green region for TLVBD0, TLVBD1, and greenish region for other glass samples. The Correlated Color Temperature (CCT) of the illuminant, which is connected to the visual acuity, emotional state, and mental well-being, was determined by using the following empirical formula given by McCamy [28], [53]:

$$CCT = 499n^3 + 3525n^2 - 6823n + 5520 \quad (11)$$

Where, $n = \frac{x-x_e}{y-y_e}$ and epicenter (x_e, y_e) corresponds to (0.3320, 0.1858). The estimated values of CCT were reported in Table 4. These values predicted the suitability of the prepared glass matrix for indoor or outdoor applications. Glasses with CCT < 3500 K generate warm light for indoor lighting applications, 3500 K < CCT < 5000 K produce neutral white light for outdoor lighting purpose and CCT > 5000 K produce cool white light matching the daylight and are suitable for environments demanding high visibility and color accuracy. So, prepared glass samples had CCT values > 5000 K making them suitable for improving the color accuracy, enhancing visibility and improving focus, so perfect for lighting applications in educational institutions, healthcare facilities, industries, street lighting, parking lots, etc. One more parameter that gives an idea about the source's competence to yield true colors of the object, known as the Color Rendering Index (CRI), was also assessed and tabulated in Table 4.

Table 4: Color Coordinates, Y/B Ratio, CRI, CCT Values, and Emission Color of TLVBD Glass System at Excitation Wavelengths of 350 nm, 363 nm, 386 nm, and 452 nm.

Excitation Wavelength	Parameters	Sample Codes					
		TLVBD0	TLVBD1	TLVBD3	TLVBD5	TLVBD9	TLVBD10
350 nm	x-coordinate	0.333	0.349	0.335	0.304	0.305	0.348
	y-coordinate	0.366	0.368	0.358	0.333	0.328	0.374
	Y/B ratio	1.31	1.44	1.18	0.98	1.31	1.62
	CRI	88	90	95	87	76	24
	CCT (K)	5497	4928	5409	6890	6936	4973

	Emission color	Cool White	Neutral White	Cool White	Cool White	Cool White	Neutral White
363 nm	x-coordinate	0.323	0.341	0.329	0.297	0.299	0.338
	y-coordinate	0.359	0.364	0.358	0.321	0.316	0.360
	Y/B ratio	1.25	1.39	1.2	0.89	1.24	1.51
	CRI	87	89	93	90	80	30
	CCT (K)	5892	5182	5622	7541	7494	5295
	Emission color	Cool White	Cool White	Cool White	Cool White	Cool White	Cool White
386 nm	x-coordinate	--	0.324	0.315	0.284	0.301	0.339
	y-coordinate	--	0.343	0.334	0.295	0.308	0.359
	Y/B ratio	--	1.42	1.19	0.93	1.39	1.6
	CRI	--	84	87	89	80	32
	CCT (K)	--	5859	6330	9234	7455	5245
	Emission color	--	Cool White	Cool White	Cool White	Cool White	Cool White
452 nm	x-coordinate	0.352	0.348	0.325	0.304	0.329	0.354
	y-coordinate	0.493	0.472	0.442	0.411	0.419	0.422
	Y/B ratio	0.46	0.38	0.27	0.26	0.61	1.2
	CCT (K)	5098	5149	5709	6435	5600	4917
	Emission color	Cool White	Cool White	Cool White	Cool White	Cool White	Neutral White

Table 5: Comparison of PL Parameters of TLVBD Glass System with Already Published Work

Sample Code	Excitation Wavelength (nm)	Y/B Ratio	CIE (x, y)	CCT (K)	Reference
ZLVBD1	386	1.18	(0.29, 0.286)	9006	[4]
0.5 Dy^{3+}: LZB	386	1.6	(0.34, 0.36)	5104	[7]
Glass A	384	0.79	(0.30, 0.34)	7089	[9]
DPNAB (x=0)	385	1.3	(0.33, 0.37)	5761	[48]
LABD-4	387	1.08	(0.34, 0.39)	5260	[59]
TLVBD1	386	1.42	(0.32,0.34)	5859	This work
TLVBD3	386	1.19	(0.32,0.33)	6330	This work
TLVBD10	386	1.6	(0.34,0.36)	5245	This work

4. Conclusions

In this work, a comprehensive analysis of the physical, optical, and photoluminescence performance of pristine glass matrix $x TiO_2 \cdot (10-x) V_2O_5 \cdot 30Li_2O \cdot 60B_2O_3$ + 1 mol% Dy_2O_3 glasses (with x = 0, 1, 3, 5, 9, 10 mol%) synthesised through the melt quench method was reported. XRD confirmed the amorphous nature of the glass samples. The density calculations revealed the overall structure's compactness, decrease in inter-ionic distance, and a stronger field strength around titanium ions with increasing amount of TiO_2. FTIR spectroscopy gave an idea about the existence of TiO_4 group, TiO_6 vibrations, V=O vibration of VO_5, and borate structural units along with the Li^+ vibrations. Optical band gap varied between 0.052 eV- 2.86 eV, indicating the potential application of glass samples TLVBDx (with x =0, 1, 3, 5, 9) in IR sensors, thermal imaging, and night vision. The values of refractive index and dielectric constant revealed that TLVBD0 and TLVBD1 were suitable for optical filters and capacitors, whereas TLVBD10 was found to be suitable for anti-reflective coatings. The bonding parameter (δ) values were found positive, depicting the covalent nature of the bond shared by Dy^{3+} ions with the surrounding ligands. Low value of TPA coefficient (β_{TPA} = 13.59 cm/GW) for TLVBD10 suggested its utility in waveguides and it was found that TPA values can be managed by tuning the optical band gap. PL excitation and emission spectra were recorded for Dy^{3+} ions and demonstrated that in contrary to V_2O_5, TiO_2 enhanced the luminescence by generating more asymmetry in the lattice. The CIE coordinates, CCT, and CRI values were correlated to standard white luminescence lying in the cool white region for excitation wavelengths 350 nm, 363 nm, 386 nm, whereas they coincided with yellowish-green and green color in the cool white region for excitation wavelength 452 nm. Finally, it can be concluded that our entitled glasses were found suitable for the development of WLED devices, green LEDs, electronic devices like capacitors, and optical filters. Our study has been limited to a fixed concentration of Dy_2O_3. So, for future prospect, this series can be conducted with varying Dy^{3+} concentration to determine the optimal level for concentration quenching. Moreover, co-doping with one more RE ion such as Eu^{3+}, Ce^{3+}, or Sm^{3+} may assist in shifting emission bands and chromaticity towards targeted regions like cool white, warm white, orange, etc.

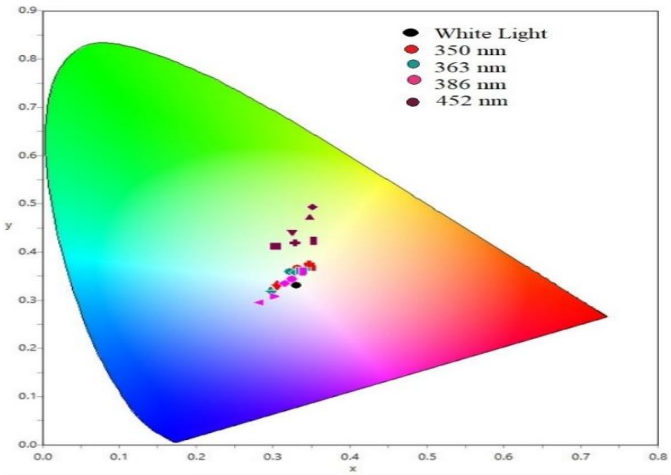

Fig. 14: 1931 CIE Chromaticity Diagram for 1 mol% Dy^{3+}-Doped TLVBDx (with x= 1,3,5,9,10 mol%) Glass Matrix excited at λ_{exc} = 350 nm, 363 nm, 386 nm, and 452 nm Wavelength depicting the closeness of Chromaticity Parameters of the Glass Samples with that of White Light (0.33,0.33).

Acknowledgments

The authors would like to thank the Central Instrumentation Laboratory (CIL), DCRUST, Murthal, for facilitating FTIR measurements. The authors also want to acknowledge DST, Delhi, for providing Fluorescence facilities under FIST Research Grant (Sanction Order No. & Date: SR/FST/PS-1/2018/32).

References

[1] S. Dalal, S. Khasa, M.S. Dahiya, A. Yadav, A. Agarwal, S. Dahiya, Optical and thermal investigations on vanadyl doped zinc lithium borate glasses, J. Asian Ceram. Soc. 3 (2015) 234–239. Available online: https://doi.org/10.1016/j.jascer.2015.03.004.

[2] S.K. Arya, M.K. Chhina, R. Choudhary, V. Dua, K. Singh, Growth of different nanocrystalline phases in ZnO–Li2O–B2O3–TiO2–V2O5 glass and their effect on photoluminescence and photocatalytic activity, Ceram. Int. 48 (2022) 20619–20626. Available online: https://doi.org/10.1016/j.ceramint.2022.04.030.

[3] G. Lakshminarayana, K.M. Kaky, S.O. Baki, A. Lira, U. Caldiño, I. V. Kityk, M.A. Mahdi, Optical absorption, luminescence, and energy transfer processes studies for Dy3+ /Tb3+-codoped borate glasses for solid-state lighting applications, Opt. Mater. (Amst). 72 (2017) 380–391. Available online: https://doi.org/10.1016/j.optmat.2017.06.030.

[4] A. Bishnoi, M. Duhan, S. Khasa, An insight into the transition metal dependent structural, optical, and electrical properties of dysprosium doped lithium zinc borate glasses, Mol. Cryst. Liq. Cryst. 0 (2023) 1–21. Available online: https://doi.org/10.1080/15421406.2023.2256577.

[5] M.A. Marzouk, S.M. Abo-Naf, H.A. Zayed, N.S. Hassan, Glass Former Effects on Photoluminescence and Optical Properties of Some Heavy Metal Oxide Glasses Doped with Transition Metal Ions, J. Appl. Spectrosc. 84 (2017) 162–169. Available online: https://doi.org/10.1007/s10812-017-0445-z.

[6] H.M. Gomaa, S.M. Elkatlawy, I.S. Yahia, H.A. Saudi, A.M. Abdel-Ghany, Influence of the gradual increase of TiO2-impurities on the structural and optical properties of some calcium sodium borate glasses, Optik (Stuttg). 244 (2021) 167543. Available online: https://doi.org/10.1016/j.ijleo.2021.167543.

[7] Luminescence - 2023 - Vijayalakshmi - Noncytotoxic Dy3+-activated glass emits cool white light for near ultraviolet-based.pdf, (n.d.).

[8] J. Dahiya, A. Hooda, A. Agarwal, S. Khasa, Tuneable colour flexibility in Dy3+ & Eu3+ co-doped lithium fluoride bismuth borate glass system for solid state lighting applications, J. Non. Cryst. Solids. 576 (2022) 121237. Available online: https://doi.org/10.1016/j.jnoncrysol.2021.121237.

[9] N. Deopa, A.S. Rao, Photoluminescence and energy transfer studies of Dy3+ ions doped lithium lead alumino borate glasses for w-LED and laser applications, J. Lumin. 192 (2017) 832–841. Available online: https://doi.org/10.1016/j.jlumin.2017.07.052.

[10] P.S. Gahlot, V.P. Seth, A. Agarwal, N. Kishore, S.K. Gupta, M. Arora, D.R. Goyal, Influence of ZnO on optical properties and dc conductivity of vanadyl-doped alkali bismuthate glasses, Radiat. Eff. Defects Solids. 159 (2004) 223–231. Available online: https://doi.org/10.1080/1042015042000209334.

[11] A. V. Deshpande, N.S. Paighan, Electrical conductivity of lithium borosilicate glasses modified with TiO2, IOP Conf. Ser. Mater. Sci. Eng. 2 (2009). Available online: https://doi.org/10.1088/1757-899X/2/1/012051.

[12] D. Prakash, V.P. Seth, I. Chand, P. Chand, EPR study of vanadyl ion in CoO · PbO · B2O3 glasses, J. Non. Cryst. Solids. 204 (1996) 46–52. Available online: https://doi.org/10.1016/0022-3093(96)00391-2.

[13] S.K. Arya, S.S. Danewalia, M. Arora, K. Singh, Effect of variable oxidation states of vanadium on the structural, optical, and dielectric properties of B2O3-Li2O-ZnO-V2O5 glasses, 2016. Available online: https://doi.org/10.1021/acs.jpcb.6b08285.

[14] S.K. Arya, G. Kaur, K. Singh, Effect of vanadium on the optical and physical properties of lithium borate glasses, J. Non. Cryst. Solids. 432 (2016) 393–398. Available online: https://doi.org/10.1016/j.jnoncrysol.2015.10.037.

[15] S.K. Arya, K. Singh, Structural and optical properties of 30Li2O-55B2O3-5ZnO-xTiO2-(10 -x)V2O5, ($0 \leq x \leq 10$) glasses, J. Non. Cryst. Solids. 414 (2015) 51–58. Available online: https://doi.org/10.1016/j.jnoncrysol.2015.02.004.

[16] A.S. Abouhaswa, H.M.H. Zakaly, S.A.M. Issa, M. Rashad, M. Pyshkina, H.O. Tekin, R. El-Mallawany, M.Y.A. Mostafa, Synthesis, physical, optical, mechanical, and radiation attenuation properties of TiO2–Na2O–Bi2O3–B2O3 glasses, Ceram. Int. 47 (2021) 185–204. Available online: https://doi.org/10.1016/j.ceramint.2020.08.122.

[17] A.M. Abdelghany, H.A. Elbatal, Effect of TiO2 doping and gamma ray irradiation on the properties of SrO–B2O3 glasses, J. Non. Cryst. Solids. 379 (2013) 214–219. Available online: https://doi.org/10.1016/j.jnoncrysol.2013.08.020.

[18] M.S. Sadeq, H.Y. Morshidy, Effect of mixed rare-earth ions on the structural and optical properties of some borate glasses, Ceram. Int. 45 (2019) 18327–18332. Available online: https://doi.org/10.1016/j.ceramint.2019.06.046.

[19] L. Murawski, C.H. Chung, J.D. Mackenzie, Electrical properties of semiconducting oxide glasses, J. Non. Cryst. Solids. 32 (1979) 91–104. Available online: https://doi.org/10.1016/0022-3093(79)90066-8.

[20] B. Tirumala Rao, B.R. Venkateswara Rao, Ch.Rajyalakshmi, G. Sridevi, M. Rajesh Yadav, G.V.L. Kanth, S. Cole, Characterization and spectroscopic investigations of zinc alumino lithium borate glasses doped with TiO2, Mater. Today Proc. (2023). Available online: https://doi.org/10.1016/j.matpr.2023.06.076.

[21] V. Kesarwani, V.K. Rai, Effect of adding TiO2 as modifier on the optical thermometric ability of tellurium tungstate glass, Mater. Res. Bull. 167 (2023) 112445. Available online: https://doi.org/10.1016/j.materresbull.2023.112445.

[22] B. Srinivas, A. Hameed, G. Srinivas, M. Narasimha Chary, M. Shareefuddin, Influence of V2O5 on physical and spectral (optical, EPR & FTIR) studies of SrO-TeO2-TiO2-B2O3 glasses, Optik (Stuttg). 225 (2021). Available online: https://doi.org/10.1016/j.ijleo.2020.165815.

[23] S. Cetinkaya Colak, Role of titanium ions on the optical and thermal properties of zinc borate glass doped with TiO2, Phys. Chem. Glas. Eur. J. Glas. Sci. Technol. Part B. 58 (2017) 41–48. Available online: https://doi.org/10.13036/17533562.57.2.067.

[24] B. V. Padlyak, I.I. Kindrat, V.T. Adamiv, I.M. Teslyuk, A. Drzewiecki, Spectroscopic properties and luminescence of the lithium tetraborate glasses co-doped with manganese and europium, Opt. Mater. (Amst). 154 (2024) 115782. Available online: https://doi.org/10.1016/j.optmat.2024.115782.

[25] P. Sai Dinesh, M. Kumar, Y.C. Ratnakaram, Impact of modifiers on structural and optical properties of Dy3+doped different lithium tetraborate glasses for W-LED applications, Infrared Phys. Technol. 136 (2024) 105029. Available online: https://doi.org/10.1016/j.infrared.2023.105029.

[26] S. Karthika, S.S. Sundari, K. Marimuthu, P. Meena, Enhancement of electrical and radiation shielding properties of vanadium doped lithium telluroborate (LTB) glasses, Chem. Phys. Impact. 8 (2024) 100430. Available online: https://doi.org/10.1016/j.chphi.2023.100430.

[27] S. Raheja, R. Singh, Modification of niobium borate glasses doped with titanium for optical applications, Mater. Today Proc. (2024). Available online: https://doi.org/10.1016/j.matpr.2024.05.033.

[28] M. Sreenivasulu, V.K. Chavan, B. Rupa Venkateswara Rao, High Density and Thermal Stability of Vanadium-Doped Glass Material for Optical Bandpass Filter, Arab. J. Sci. Eng. 48 (2023) 8035–8046. Available online: https://doi.org/10.1007/s13369-022-07414-z.

[29] C.R. Kesavulu, H.J. Kim, S.W. Lee, J. Kaewkhao, N. Wantana, S. Kothan, S. Kaewjaeng, Optical spectroscopy and emission properties of Ho3+-doped gadolinium calcium silicoborate glasses for visible luminescent device applications, J. Non. Cryst. Solids. 474 (2017) 50–57. Available online: https://doi.org/10.1016/j.jnoncrysol.2017.08.018.

[30] Z.A. Said Mahraz, M.R. Sahar, S.K. Ghoshal, Band gap and polarizability of boro-tellurite glass: Influence of erbium ions, J. Mol. Struct. 1072 (2014) 238–241. Available online: https://doi.org/10.1016/j.molstruc.2014.05.017.

[31] A.S. Alqarni, R. Hussin, S.K. Ghoshal, S.N. Alamri, Y.A. Yamusa, S.A. Jupri, Intense red and green luminescence from holmium activated zinc-sulfo-boro-phosphate glass: Judd-Ofelt evaluation, J. Alloys Compd. 808 (2019) 151706. Available online: https://doi.org/10.1016/j.jallcom.2019.151706.

[32] J. Dahiya, A. Hooda, A. Agarwal, S. Khasa, Effect of Dysprosium and Samarium RE ion Co-doping on photoluminescence behaviour of novel alkali fluoride bismuth borate glasses: A white LED material, Opt. Mater. (Amst). 134 (2022) 113162. Available online: https://doi.org/10.1016/j.optmat.2022.113162.
[33] V. Attri, S. Khasa, Structural, Electrical and Optical Analysis of Barium Boro-Bismuthate Glass System: Opto-Electronic Devices, ECS Trans. 107 (2022) 10957–10967. Available online: https://doi.org/10.1149/10701.10957ecst.
[34] R. Rohilla, M.S. Dahiya, A. Agarwal, S. Khasa, Influence of Sr2+ ions on structural, optical and bioactive behaviour of phosphoborate glass system, J. Mol. Struct. 1291 (2023) 136095. Available online: https://doi.org/10.1016/j.molstruc.2023.136095.
[35] R. Rohilla, M.S. Dahiya, A. Hooda, A. Agarwal, S. Khasa, Effect of Li+ ions on structural, optical and nano-crystallization behaviour of Na2O-CaO-P2O5-B2O3 glass system: Biomedical applications, J. Non. Cryst. Solids. 593 (2022) 121774. Available online: https://doi.org/10.1016/j.jnoncrysol.2022.121774..
[36] V. Attri, M.S. Dahiya, R. Kumar, A. Hooda, A. Agarwal, S. Khasa, Electrical, optical and high energy radiation shielding study of TMI-doped multi-component glasses, J. Mater. Sci. Mater. Electron. 34 (2023) 1–16. Available online: https://doi.org/10.1007/s10854-023-10625-1.
[37] G.P. Singh, J. Singh, P. Kaur, T. Singh, R. Kaur, S. Kaur, D.P. Singh, Impact of TiO2 on radiation shielding competencies and structural, physical and optical properties of CeO2–PbO–B2O3 glasses, J. Alloys Compd. 885 (2021) 160939. Available online: https://doi.org/10.1016/j.jallcom.2021.160939.
[38] M. Malik, A. Khatri, A. Hooda, M.S. Dahiya, S. Khasa, Structural, spectroscopic and electrical properties of iron doped oxyfluoride bismuth borate glasses, Mater. Res. Bull. 162 (2023) 112182. Available online: https://doi.org/10.1016/j.materresbull.2023.112182.
[39] S.Y. Marzouk, M.A. Azooz, H.M. Elsaghier, Structural and optical properties of barium titanium borate glasses doped with ytterbium, J. Mater. Sci. Mater. Electron. Available online: https://doi.org/10.1007/s10854-022-08665-0.
[40] P.N. Rao, C. Laxmi Kanth, D. Krishna Rao, N. Veeraiah, Influence of titanium ions on optical properties of AF–PbO–B2O3 glasses, J. Quant. Spectrosc. Radiat. Transf. 95 (2005) 373–386. Available online: https://doi.org/10.1016/j.jqsrt.2004.11.005.
[41] Y.S.M. Alajerami, S. Hashim, W.M.S. Wan Hassan, A.T. Ramli, the effect of titanium oxide on the optical properties of lithium potassium borate glass, J. Mol. Struct. 1026 (2012) 159–167.Available online: https://doi.org/10.1016/j.molstruc.2012.05.047.
[42] Manjeet, Ravina, Amit, K. Poria, N. Deopa, A. Kumar, R.P. Chahal, Optimization of dysprosium ions doped borate glasses for photoluminescence applications, Mater. Lett. X. 19 (2023) 100208. Available online: https://doi.org/10.1016/j.mlblux.2023.100208.
[43] T.A. Taha, Y.S. Rammah, Optical characterization of new borate glass doped with titanium oxide, J. Mater. Sci. Mater. Electron. 27 (2016) 1384–1390. Available online: https://doi.org/10.1007/s10854-015-3901-7.
[44] S.G. Motke, S.P. Yawale, S.S. Yawale, Infrared spectra of zinc doped lead borate glasses, Bull. Mater. Sci. 25 (2002) 75–78. Available online: https://doi.org/10.1007/BF02704599.
[45] S. Rada, E. Culea, M. Rada, P. Pascuta, V. Maties, Structural and electronic properties of tellurite glasses, J. Mater. Sci. 44 (2009) 3235–3240. Available online: https://doi.org/10.1007/s10853-009-3433-8.
[46] J. HEMATYAR, H. RASHIDI, M. ZAKERKISH, S.P. PAYAMI, S.B. GHADERIAN, Original paper Original paper, Maedica A J. Clin. Med. 17 (2022) 1929–1938. https://doi.org/10.26574/maedica.2022.17.4.762.
[47] P. Narwal, M.S. Dahiya, A. Yadav, A. Hooda, A. Agarwal, S. Khasa, Dy3+ doped LiCl–CaO–Bi2O3–B2O3 glasses for WLED applications, Ceram. Int. 43 (2017) 11132–11141. Available online: https://doi.org/10.1016/j.ceramint.2017.05.160.
[48] J. Dahiya, A. Hooda, A. Agarwal, S. Khasa, Detailed optical analysis of Dy3+ and Pr3+ co-doped alumino-borate glasses for visible lighting applications, Ceram. Int. 49 (2023) 15284–15294. Available online: https://doi.org/10.1016/j.ceramint.2023.01.112.
[49] W.T. Carnall, P.R. Fields, K. Rajnak, Electronic energy levels of the trivalent lanthanide aquo ions. III. Tb3+, J. Chem. Phys. 49 (1968) 4412–4423. Available online: https://doi.org/10.1063/1.1669892.
[50] H.A. Thabit, A.K. Ismail, G. Jagannath, A. I. , S. Hashim, M.I. Sayyed, Physical, optical and spectroscopic characteristics investigation for doped Dy3+ borate glass matrix, J. Non. Cryst. Solids. 608 (2023) 122258. Available online: https://doi.org/10.1016/j.jnoncrysol.2023.122258.
[51] M. Taj S., C. Devaraja, U. Deka, A review of boron oxide glasses infused with individual oxides of lanthanide elements: For their physical, structural, optical, and gamma shielding properties, J. Alloys Compd. 1010 (2025) 178279. Available online: https://doi.org/10.1016/j.jallcom.2024.178279.
[52] K. Kowalska, J. Pisarska, W.A. Pisarski, Yb3+-Doped Titanate–Germanate Glasses for Near-IR Luminescence Applications: Synthesis, Characterization, and the Influence of TiO2 Concentration, Materials (Basel). 17 (2024). Available online: https://doi.org/10.3390/ma17235874.
[53] M.K. Halimah, M.N. Ami Hazlin, F.D. Muhammad, Experimental and theoretical approach on the optical properties of zinc borotellurite glass doped with dysprosium oxide, Spectrochim. Acta - Part A Mol. Biomol. Spectrosc. 195 (2018) 128–135. Available online: https://doi.org/10.1016/j.saa.2017.12.054.
[54] P. Srilakshmi, A. Uma Maheswari, V. Sajeev, M. Sivakumar, Tuning the optical bandgap of V2O5 nanoparticles by doping transition metal ions, Mater. Today Proc. 18 (2019) 1375–1379. Available online: https://doi.org/10.1016/j.matpr.2019.06.603.
[55] T. Wang, T. Xu, Effects of vanadium doping on microstructures and optical properties of TiO2, Ceram. Int. 43 (2017) 1558–1564. Available online: https://doi.org/10.1016/j.ceramint.2016.10.132.
[56] E. Radha, D. Komaraiah, R. Sayanna, J. Sivakumar, Influence of dysprosium ions on structural, optical, luminescence properties and photocatalytic ability of spin coated dysprosium ions doped TiO2 thin films, Thin Solid Films. 761 (2022) 139519. Available online: https://doi.org/10.1016/j.tsf.2022.139519.
[57] L.H.C. Andrade, S.M. Lima, A. Novatski, A.M. Neto, A.C. Bento, M.L. Baesso, F.C.G. Gandra, Y. Guyot, G. Boulon, Spectroscopic assignments of Ti3+ and Ti4+ in titanium-doped OH- free low-silica calcium aluminosilicate glass and role of structural defects on the observed long lifetime and high fluorescence of Ti3+ ions, Phys. Rev. B - Condens. Matter Mater. Phys. 78 (2008). Available online: https://doi.org/10.1103/PhysRevB.78.224202.
[58] A.S. Alqarni, I. Bulus, I.M. Danmallam, N.N. Yusof, Enhanced spectroscopic traits of Eu3+/Dy3+ co-doped doro-telluro-borate glasses: Effect of silver nanoparticles embedment, J. Non. Cryst. Solids. 608 (2023). Available online: https://doi.org/10.1016/j.jnoncrysol.2023.122238.
[59] P.P. Pawar, S.R. Munishwar, S. Gautam, R.S. Gedam, Physical, thermal, structural and optical properties of Dy3+ doped lithium alumino-borate glasses for bright W-LED, J. Lumin. 183 (2017) 79–88. https://doi.org/10.1016/j.jlumin.2016.11.027.